Electronic Supplementary Material (ESI) for Lab on a Chip.

Subsurface to substrate: dual-scale micro/nanofluidic networks for investigating transport anomalies in tight porous media

Shaina A. Kelly, Carlos Torres-Verdín, and Matthew T. Balhoff *

Department of Petroleum and Geosystems Engineering, The University of Texas at Austin, Austin, TX 78712
Contribution from the Center for Nano- and Molecular Science, The University of Texas at Austin, Austin, TX 78712

Corresponding Author:

Matthew T. Balhoff
The University of Texas at Austin
CPE 4.182A, 200 E. Dean Keeton
Austin, TX 78712
Tel: 512-471-3246
Email: balhoff@mail.utexas.edu

Supporting Information

Pictures from the Dual-Scale Micro/Nanofluidic Network Fabrication Workflow

These following compilation of photos from our fabrication process are intended to aid those replicating the process.

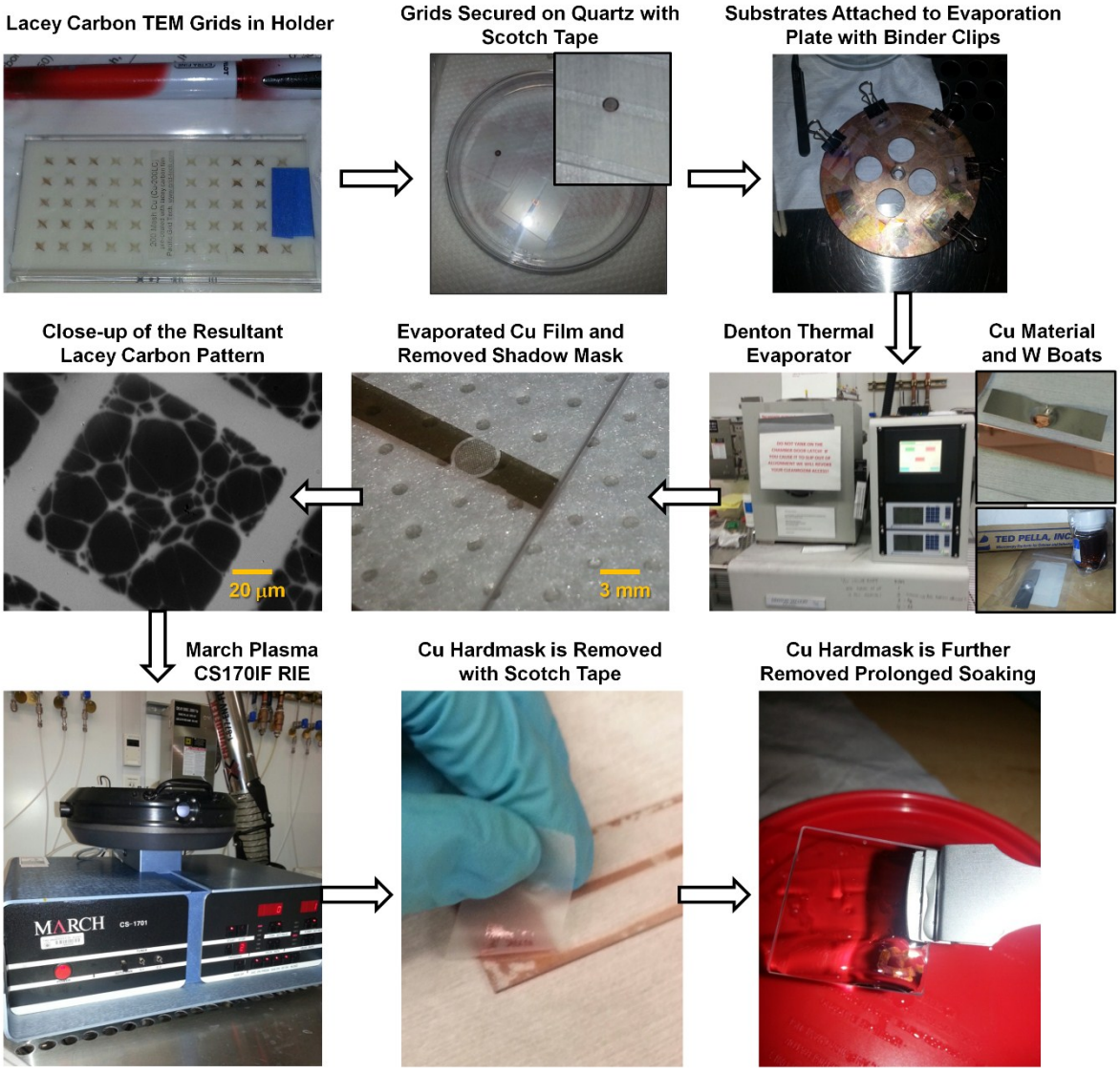

Fig. S1. Photos of the main steps of the dual-scale micro/nanofluidic network fabrication process.

Reactive Ion Etch Recipe Tuning

Reactive ion etch (RIE) recipe tuning with the March Plasma CS170IF revealed that higher radio frequency (RF) power and longer chamber times resulted in better quality etching.

Table S1: CF_4 Reactive Ion Etch Recipe Results with a March Plasma CS170IF

Trial ID	t (s)	CF_4 Flow Rate (sccm)	Base Pressure (mTorr)	RF Power (W)	Etch Quality
A	**120**	10.5	80	**200**	Poor
B	**120**	10.5	80	**250**	Good
C	**120**	10.5	80	**300**	Good
D	**240**	10.5	80	**150**	Poor
E	**240**	10.5	80	**200**	Good

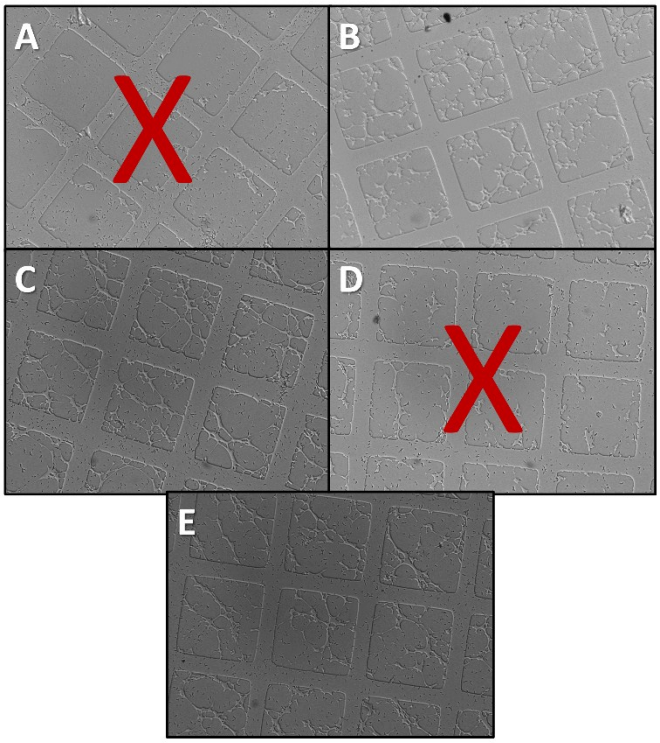

Fig. S2. Results of different RIE etching formulas as indicated in Table S1. Letters correspond to the Trial IDs and red X marks indicate plasma etching formulas that were not successful (as demonstrated in the corresponding image).

Scanning Electron Microscope Imaging Parameters

The scanning electron microscopes (SEMs) used were a JEOL SEM JSM-6490 and a FEI XL30 Environmental-SEM. The former was used in high vacuum mode only and the latter was used in both

high vacuum and low vacuum (at a pressure of ~ 0.1-0.3 torr) modes. The detectors used in high vacuum mode were the Everhart-Thornley and the BSE detectors and the GSED was used in low vacuum mode. When viewing in high vacuum mode a thin layer of gold was deposited on the samples with a Denton Gold Sputter unit. The sputter time for the gold film ranged from 15-60 s among the samples; we conjectured that a thinner layer of gold may be best since the thickness of the deposited gold layer is on a similar order of thickness to that of the nano-structures. For the low vacuum mode no ancillary sample preparation was needed.

In regard to imaging settings we viewed the samples at a range of accelerating voltages (5-30 kV) and spot sizes (30 - 90 nm) and found, to our initial surprise, that visualization of the sample was extremely difficult at high accelerating voltages and small spot sizes, settings characteristic of high resolution imaging. This may be because the investigation volume of incident electrons increases with stronger beam energy or accelerating voltage. A larger depth of investigation potentially equates to less signal from the thin surface features which are ~ 20 nm high features in this case. A smaller spot size can equate to gaps between dwell points where signal is not generated (perceived graininess). This graininess was especially pronounced with the thin film nano-structures. Indeed, looking into the literature, most papers featuring thin film type SEM images use accelerating voltages on the order of 5 kV and very small working distances (1). Likewise, we found images improved at shorter working distances, but we were limited in this parameter when desiring to tilt the sample. The maximum tilt we were able to achieve was 45˚ (in the JEOL). It was hoped semi cross sections of some of the nanochannel networks could be gleamed in tilted views, but due to the shallowness of the structures, there was only moderate success with this goal. We found the optimum parameters for imaging the thin film nano-structures to be an accelerating voltage of ~10 kV, a spot size of 60 nm +, and a working distance of 10 mm or less. Additional techniques that improved the image quality were the use of Aperture 1, the smallest aperture, in the JEOL and using a cleaner pole piece in the frequently used FEI.

Alternate Fabrication Approach with Plasma Enhanced Chemical Vapor Deposition

We also explored using a bottom-up instead of top-down procedure (reactive ion etching [RIE] is a top-down procedure) for master creation. Specifically, we anisotropically deposited a thin film of silicon dioxide, SiO_2, on top of the substrate and copper mask, aiming to seal the copper in place and achieve a glassy, hydrophilic surface that did not compromise the nanochannel networks. This process was attempted with an Oxford Instruments PlasmaLab 80+ plasma enhanced chemical vapor deposition (PECVD) system and the SiO_2 deposition rate used was approximately 60 nm/min. However, this method was riddled with complications mainly due to non-conformal coating or the “bread-loafing” effect, where the diffusive arrival of atoms in the PECVD process amass thicker in areas in mask areas with high angles of arrival (such as flat surfaces and convex corners) (2); we refer readers to the Fig.’s S3-S6 for SEM images of these results. We recommend the use of chrome instead of copper (chrome adhesion to glass is far stronger than copper) in future attempts on this method. If one desires to use the master patterns themselves as lab-on-a-chip devices, a potential option is to integrate the discussed bottom-up and top-down procedures: that is, utilize PECVD to alter surface chemistry by depositing a thin oxide film after etching into the glass substrate and lift off the copper pattern. Some obstacles to this approach that we encountered are described below.

Copper Oxidation. The SEM images further revealed that the copper-based nanochannel networks are subject to oxidation. The reaction formulas for this process are as follows:

$$4Cu + O_2 \rightarrow 2Cu_2O \quad (S1)$$

As well as the higher oxide of copper, formed by heating copper in air,

$$2Cu + O_2 \rightarrow 2CuO \quad (S2)$$

In the samples where this occurred, darkened patches (oxidized areas) were apparent on the bulk of the copper film even to the naked eye. It was unclear if the oxidation initially occurred during the fabrication methods or during extended exposure to the ambient atmosphere. This oxidation may have compromised the nanochannel structures, potentially rendering the nanochannel apertures glassy and non-distinct. Methods to avoid this oxidation include: performing the thermal evaporation at high vacuum pressures (mid-10^{-5} to 10^{-6} torr) to minimize air in the instrument chamber; performing all fabrication tasks sequentially within one session to eliminate time for ambient air oxidation; and to avoid using O_2 gas in the etching process formulas.

Hillocks. Hillock structures appear in both the isotropic copper thin film deposition step and the anistropic SiO_2 film deposition step. In the former they appear as small clusters of nano-crystals and in the latter they appear as domes. Fig. S3 displays examples of such domes. The clusters of nano-crystals are hypothesized to be an artifact of the copper and not gold sputter because no distinct correlation was seen between gold sputter time and appearance of crystalline nano-structures in the SEM; still, gold is not ruled out as a candidate for the structures. The most probably mechanism for clusters of nano-crystals is a dewetting of the deposited metal films from the underlying substrates. A possible solution to minimize these structures is slower deposition rates (3), thinner overall films (shorter deposition time), and higher vacuums in the thermal evaporation chamber. In SiO_2 film deposition, these hillocks are a product of substrate-dependent crystalline structures as well as the radio-frequency (RF) power of the tool; the higher the RF power the larger the hillocks (4). Hillocks structures of the copper can be removed with RIE and lift off of the copper. However, hillocks in the SiO_2 will lead to improper glass-glass bonding, a subsequent and crucial step of the fabrication process.

SiO_2 Coating Quality. The SEM images taken of samples where a SiO_2 coating is applied suggest that this coating in non-conformal and adheres to the nanochannel networks and micro-grid at a faster rate than the copper. This poor step coverage may be due to the "bread-loafing" effect, where the diffusive arrival of atoms in the PECVD process amass thicker in areas in areas with high angles of arrival (such as flat surfaces and convex corners) (2). The result is an overhang-like structure, or "bread-loaf edge" at step edges; however, this effect usually leads to channel filling in samples where the nanochannels are taller than they are wide (5), which is the opposite case of the samples used in this work. A preferential adherence to the glass rather than the copper is also possible. A potential solution for the non-conformal films is to deposit thinner films of SiO_2, but this may lead to difficulties with subsequent bonding steps. Based on the SEM analysis results, we feel the best use for the PECVD thin film coating for the intended application is to initially deposit a thin film of SiO_2 onto a plain, clean glass slide. The purpose of this is

to make the material properties of the substrate uniform, as glass has other oxide-forming trace elements in it which can adversely affect the quality of the reactive ion etching process, as is discussed next.

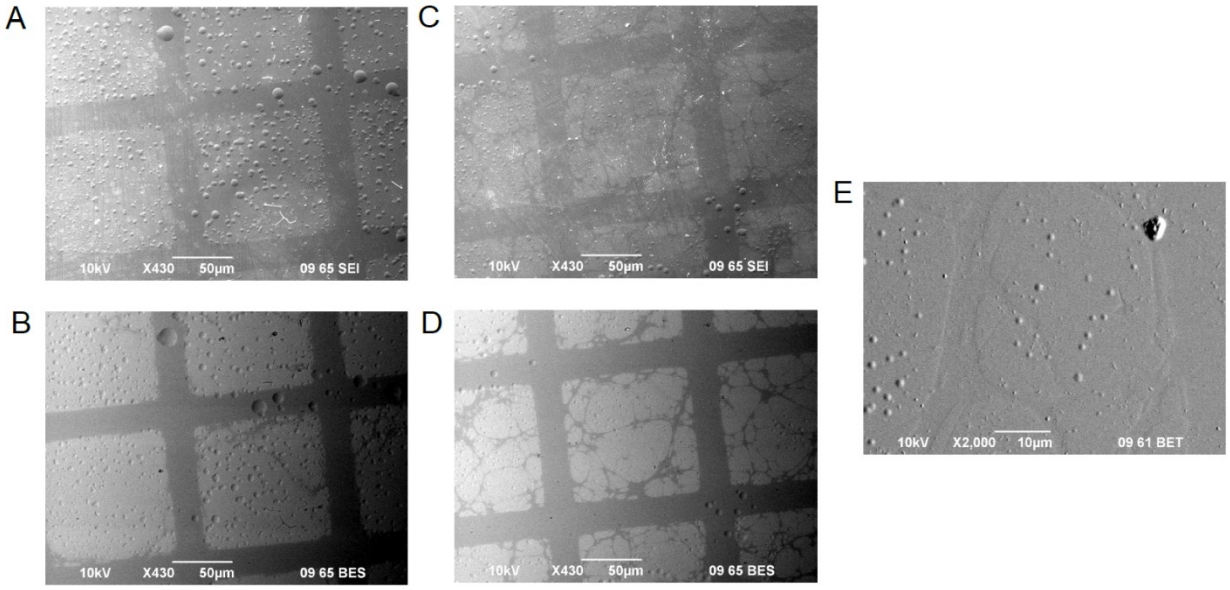

Fig. S3. Sample 2. Preparation: Glass + 20 nm Cu + 35 nm SiO_2 + 60s Au coat; Instrument: JEOL (high vacuum mode). **(A)** and **(C)** SE-SEM images of a sample exposed to the PECVD process. The channels appear to be completely covered with the glassy film and dome-like hillock structures, artifacts of PECVD, are apparent. **(B)** and **(D)** BSE-SEM (Shadow) images of the same locations featured in the SE-SEM images reveal submerged nanochannel networks since the BSE investigation volume of the impinging electrons is deeper. **(E)** Close-up view with BSE-SEM (Topo) reveals that there are some relief structures in the sample, though very faint.

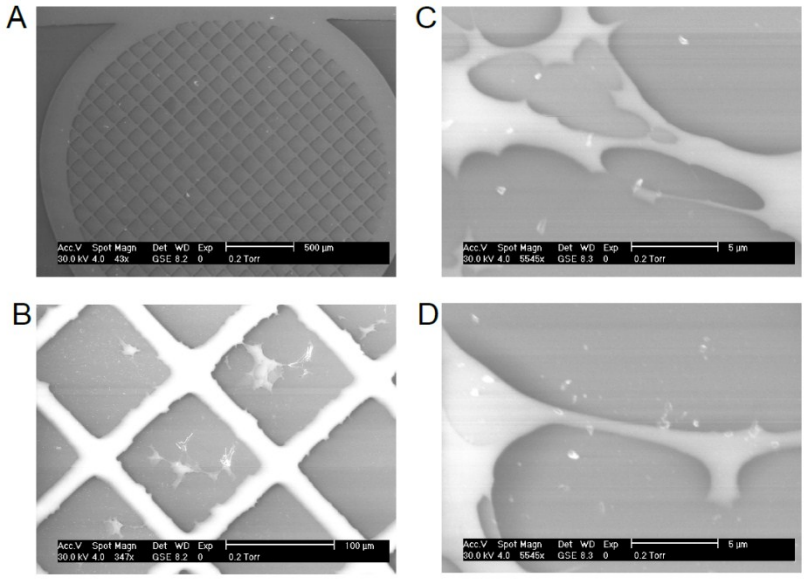

Fig. S4. Sample 3. Preparation: Glass + 20 nm Cu + 60 nm SiO_2; Instrument: FEI (low vacuum mode with a clean pole-piece). **(A)** There is a lack of GSE-SEM visible nanochannels and the micro-grid appears higher than the

copper (potentially an illusion due to relatively greater electron scatter in those areas). **(B)** Closer inspection reveals some larger network-like structures, but these structures are sparse. **(C)** and **(D)** High magnification views of the structures and their brighter color suggests that they are raised above the copper (gray background). All images were taken with the GSE detector and the substrate appears particularly "smooth", which, again, is potentially a misrepresentation caused by the weakened detected electron signal in low vacuum mode.

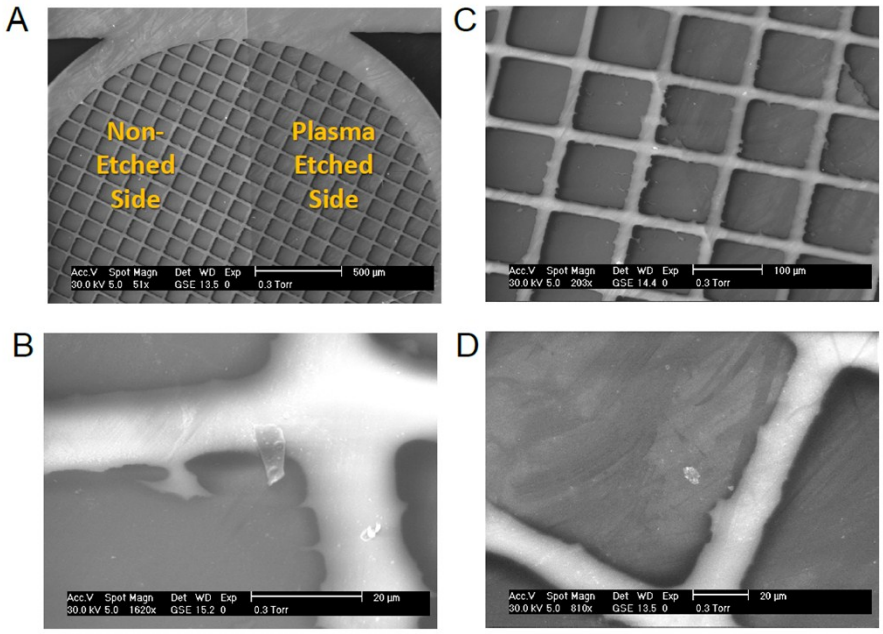

Fig. S5. Sample 4. Preparation: Glass + 20 nm Cu + 60 nm SiO_2 + 4 min of O_2+CF_4 RIE treatment on half of the sample**;** Instrument: FEI (low vacuum mode with a clean pole-piece). **(A)** and **(C)** The effect of plasma etching is apparent, but nanochannel-networks are yet to be revealed. **(B)** The orientation of a piece of debris on the non-etched side confirms that the micro-networks are raised. **(D)** The plasma etching creates a "wind-blown" effect on the sample; it is evident that more than 4 minutes of etching time is necessary.

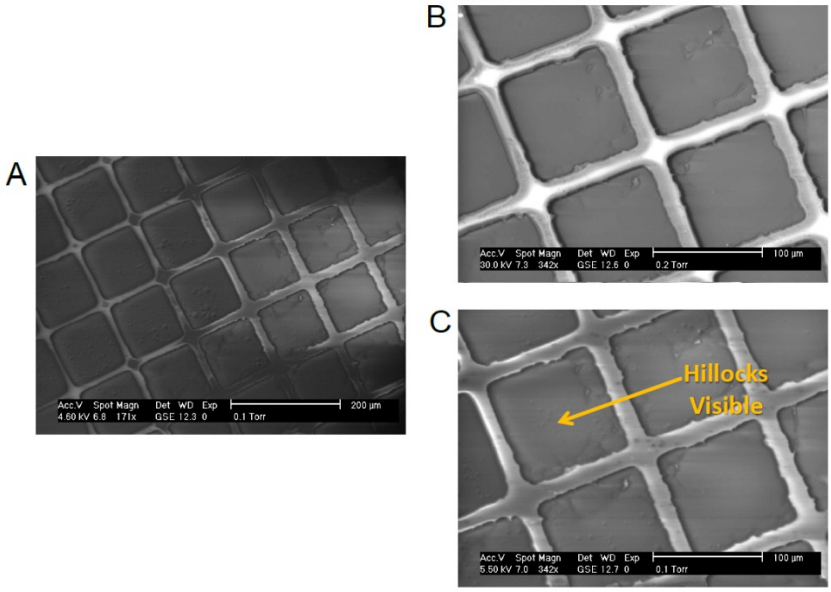

Fig. S6. Sample 5. Preparation: Glass + 30 nm Cu + 4 min of O_2+CF_4 RIE treatment on half of the sample**;** Instrument: FEI (low vacuum mode with a clean pole-piece). **(A)** There is a difference in grid appearance between the etched (right) and non-etched sides (left), especially in terms of hillocks. **(B)** and **(D)** The accelerating voltage used is highly influential on the surface structures seen on the sample as evidenced by the fact that hillocks appear when switching from 30 kV to 5.5 kV, respectively. Below 4 kV signal quality significantly declined.

Agarose

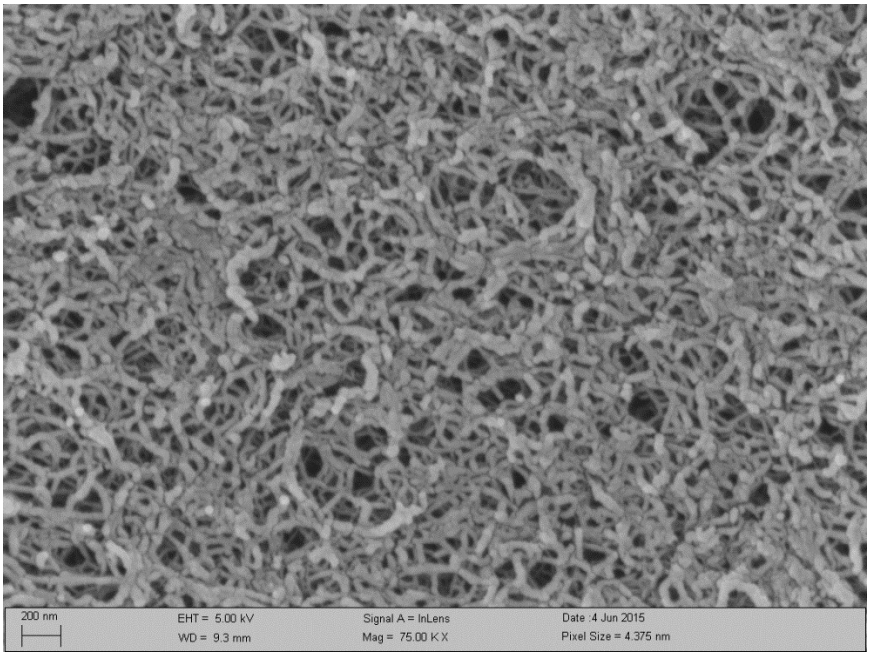

Fig. S7. A high resolution SEM image of a 2% agarose (diameter of pores is approximately 90 nm) dried with a Tousimis Samdri 790 critical point drier and imaged with a working distance of 9.3 mm and an accelerating voltage of 5 kV reveals a highly nanoporous network.

References

1. Banyamin ZY, Kelly PJ, West G, Boardman J (2014) Electrical and Optical Properties of Fluorine Doped Tin Oxide Thin Films Prepared by Magnetron Sputtering. *Coatings* 4(4):732–746.

2. Franssila S (2010) *Introduction to Microfabrication* (John Wiley & Sons).

3. Bordo K, Rubahn H-G (2012) Effect of Deposition Rate on Structure and Surface Morphology of Thin Evaporated Al Films on Dielectrics and Semiconductors. *Mater Sci* 18(4). doi:10.5755/j01.ms.18.4.3088.

4. Chung C-K, Tsai M-Q, Tsai P-H, Lee C (2005) Fabrication and characterization of amorphous Si films by PECVD for MEMS. *J Micromechanics Microengineering* 15(1):136.

5. Dumais P, Callender CL, Ledderhof CJ, Noad JP (2006) Monolithic integration of microfluidic channels, liquid-core waveguides, and silica waveguides on silicon. *Appl Opt* 45(36):9182–9190.